

Enhanced coherency of thermal emission: Beyond the limitation imposed by delocalized surface waves

Nir Dahan, Avi Niv, Gabriel Biener, Yuri Gorodetski, Vladimir Kleiner, and Erez Hasman

Micro and Nanooptics Laboratory, Faculty of Mechanical Engineering, and Russel Berrie Nanotechnology Institute, Technion—Israel Institute of Technology, Haifa 32000, Israel

(Received 13 February 2007; revised manuscript received 15 May 2007; published 27 July 2007)

Is it possible to achieve thermal radiation excited by surface waves having a coherence length much larger than what one might anticipate from the behavior of surface waves on a flat interface? We demonstrate an extraordinary coherent thermal radiation from coupled resonant cavities; each of them supports standing wave surface polaritons. The coupling is implemented by surface standing waves between the cavities. As a result, the spatial coherence length is increased by an order of magnitude compared with that of delocalized surface waves.

DOI: [10.1103/PhysRevB.76.045427](https://doi.org/10.1103/PhysRevB.76.045427)

PACS number(s): 78.68.+m, 44.40.+a, 42.72.Ai, 71.36.+c

I. INTRODUCTION

Surface waves have been shown to play a key role in spontaneous thermal emission in the near field, and dramatically affect the local density of states (DOS) in the vicinity of an interface, as well as the coherence properties of the nonradiative field.^{1–8} The spatial coherence of the thermally excited electromagnetic fields in the near field was investigated by Carminati and Greffet.⁷ It has been shown that thermally excited delocalized surface waves yield a long-range spatial coherence length L_c on a scale of the surface wave propagation length $L_{||}$, which can be much larger than the emitted wavelength $L_c \approx L_{||} \gg \lambda$.^{7,8} The near field coherence of the delocalized nonradiative surface waves was transferred into radiative fields by introducing a shallow grating on the surface.⁹ Such a grating introduced a smooth perturbation on the surface while maintaining the dynamics of the delocalized surface waves. It was found that the coherence length of the coupled radiative fields was *limited* by the spatial coherence of the delocalized surface waves ($l_c \leq L_c$).^{9,10} In light of these results, this paper addresses the question: Is it possible to overcome this *limitation* by modifying the dynamic properties of the surface waves, i.e., to achieve a coherence length of the radiative fields substantially larger than the coherence of the delocalized surface waves, such that $l_c \gg L_c$?

The physical phenomena associated with coupled resonant cavities raises the possibility of modifying and controlling well-known surface excitations such as surface plasmons and surface phonon-polaritons.^{11,12} Coupled resonator cavities are ubiquitous and can be tracked back to Lord Rayleigh's "Theory of Sound," where it was pointed out that under resonant conditions, acoustic energy is concentrated in cylindrical holes.¹³ In 1944, in his "Theory of Diffraction by Small Holes," Bethe investigated the problem of the mutual excitation of cavities coupled by small holes.¹⁴ In the early 1980s, Rendell and Scalapino studied local surface plasmons confined by microstructures.¹⁵

In this paper, we experimentally observed and analyzed extraordinary coherent thermal radiation that overcomes the coherence limitation imposed by delocalized surface waves. This resonant enhancement is due to coherent coupling be-

tween resonant cavities obtained by surface standing waves, in which each cavity supports standing wave-coupled surface polaritons. Coupled resonant cavities (CRCs) increase the photonic DOS due to thermal excitation of localized surface mode at the resonant frequency supported by the cavities, along with a coupling of the resonant mode into a radiative field. As a result, the spatial coherence length is increased by an order of magnitude compared with the coherence length of the delocalized surface waves. The resonant frequency of the radiative field is strongly dependent on the standing wave's condition inside the cavities and radiates only in a specific direction. In contrast, thermal emission obtained by coupling of delocalized surface waves has a rainbow like frequency behavior, i.e., each frequency is emitted in a different direction, one that satisfies momentum conservation.⁹

To implement the enhanced coherency, we studied the thermal radiation of CRC structures etched on an amorphous fused silica (SiO_2) substrate. A quasimonochromatic and highly directional thermal emission in the normal direction was obtained for TM polarization state due to surface phonon-polariton (SPP) excitation. The spatial coherence of the radiative field was measured to be 32λ ; more than an order of magnitude greater than the coherence length of the delocalized surface phonon polariton (SPP), which is only $\sim 2\lambda$. This generic behavior is also confirmed for silicon-carbide (SiC), which has a high delocalized SPP coherence length of 55λ . Extraordinary spatial coherence of 440λ was obtained for the radiative field of the CRCs, along with enhanced temporal coherence having a quality factor $Q \approx 500$.

II. EXPERIMENTAL RESULTS AND ANALYSIS

We studied the thermal excitation of CRCs embedded in a SiO_2 substrate in the infrared spectrum, particularly in the vicinity of $9 \mu\text{m}$ wavelength. At this wavelength the permittivity is $\epsilon(\lambda=8.93 \mu\text{m}) = \epsilon' + i\epsilon'' = -3.285 + i1.371$,¹⁶ which assures the existence of SPPs. A 30 mm in diameter periodic cavity structure was formed on SiO_2 substrate using photolithographic techniques.¹⁷ An atomic force microscope (AFM) image of the obtained periodic cavities is shown in the inset of Fig. 1(a) with periodicity $\Lambda = 8.9 \mu\text{m}$, fill factor

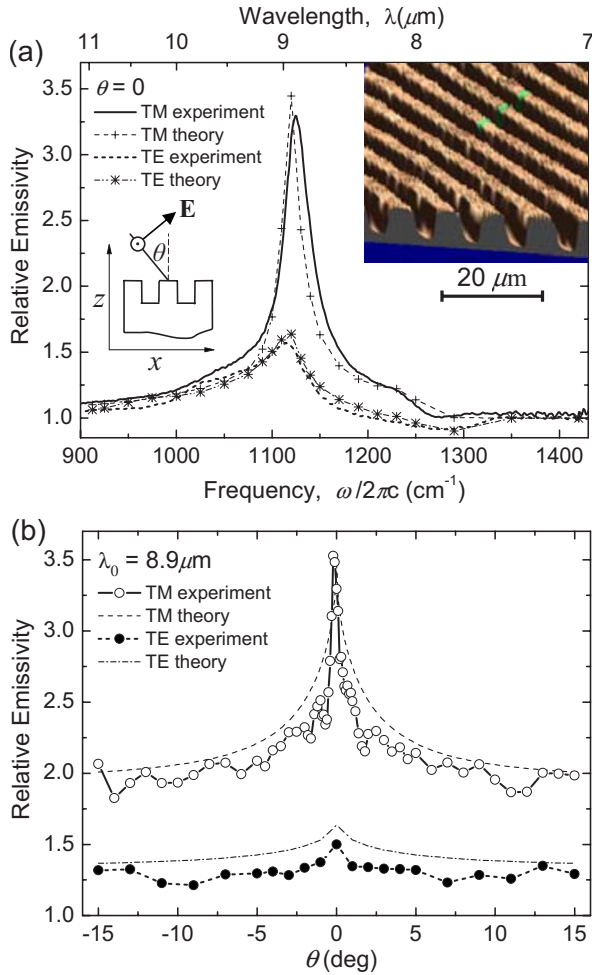


FIG. 1. (Color online). Measured and calculated relative emissivity of SiO₂-CRCs for TM and TE polarization states as a function of (a) the emitted frequency at normal direction and (b) the observed angle, at $\lambda_0 = 8.9 \mu\text{m}$. The CRC's parameters: periodicity $\Lambda = 8.9 \mu\text{m}$, fill factor $q = 0.54$, and depth $h = 2.7 \mu\text{m}$. The upper right inset in (a) shows an AFM image of the CRCs. The left inset shows the grating geometry with a coordinate system.

$q = 0.54$, and depth $h = 2.7 \mu\text{m}$. Spectral measurements of the thermal emission were performed using an infrared Fourier transform spectrometer (Vertex 70, Bruker, spectral resolution 2 cm^{-1}) equipped with a cooled HgCdTe detector. In this experiment, the sample was heated to $373 \pm 1 \text{ K}$ and a spatial filter determined the angular resolution to be about 0.6° . Figure 1(a) shows the measured and the calculated spectral relative emissivity for TM and TE polarization states in the normal emission direction. Relative emissivity is defined as the emissivity of the CRC structure normalized by the emissivity of a flat surface, for each frequency, direction, and polarization. Based on Kirchoff's law, the emissivity and the reflectivity are linked by $\tilde{\epsilon} = 1 - R$. Accordingly, the calculation of the relative emissivity was derived from the reflectivity using rigorous couple wave analysis (RCWA). A narrow spectral peak, $\Delta\tilde{\omega} = 37 \text{ cm}^{-1}$ ($\Delta\lambda = 300 \text{ nm}$), was observed only for TM polarization around $\tilde{\omega}_0 = 1124 \text{ cm}^{-1}$ ($\lambda_0 = 8.9 \mu\text{m}$) having a quality factor $Q = \omega_0/\Delta\omega \approx 30$ ($\tilde{\omega}$ is defined as $\tilde{\omega} = \omega/2\pi c$, where ω is the angular frequency and c is the speed

of light in a vacuum). A peak value of 3.5 was measured, which corresponds to an absolute emissivity of 0.98 at this frequency. This resonance spectral peak is attributed to the excitation of SPPs. The small variation from the theory is referred to structural imperfections and the temperature dependence of the SiO₂ refractive index.

The measured and calculated angular emission of the CRCs is shown in Fig. 1(b) for TM and TE polarization states at the peak frequency shown in Fig. 1(a). A narrow angular lobe was observed only for the TM polarized field. This lobe width at half maximum $\Delta\theta \approx 1.75^\circ$ is the signature of the spatial coherence length of the radiative field. The actual spatial coherence length is derived by $l_c \approx \lambda_0/\Delta\theta \approx 32\lambda_0 \approx 300 \mu\text{m}$. This value is much larger than the coherence length of a classical Lambertian thermal source $\lambda/2$.¹⁸ Moreover, it is significantly higher than the predicted coherence length of the nonradiative field on a SiO₂-vacuum flat interface L_c . The coherence length can be evaluated by the propagation distance of delocalized SPPs on the interface, which is $L_c \approx L_{\parallel} \approx 1/\text{Im}(k_{\parallel}) = 17 \mu\text{m} \approx 2\lambda_0$, where $k_{\parallel} = \omega/c\sqrt{\epsilon(\omega)/[\epsilon(\omega)+1]}$ is the SPPs wave number.⁷ This is the first time that we are aware of that the spatial coherence length of the radiative field is greater than the predicted coherence length of delocalized surface waves ($l_c \gg L_{\parallel}$). Note that by the use of a shallow grating upon SiO₂, we recently obtained a very low coherence thermal emission at the same frequency $\tilde{\omega}_0$.¹⁷ The emission distribution can be viewed as the result of the interplay between two mechanisms. The first increases the DOS due to localized modes associated with standing wave inside the cavity originated by coupled SPPs.¹⁹ The second couples between adjacent resonant cavities achieved by surface standing waves. As a result, the resonant mode supported by the cavity is coupled into the radiative field according to the structure periodicity^{20,21} and interferes constructively to obtain a coherent emission. Since surface waves do not exist for TE polarization, there is no coupling between the cavities in this case, i.e., directional emission would not be observed. Indeed, the TE polarization exhibits a broad angular emission enhancement resulting from a geometric resonance;^{22,23} see Fig. 1(b).

Figure 2(a) shows calculated reflectivity as a function of the cavity depth for TM polarization for two illuminating wavelengths $\lambda_0 = 8.9 \mu\text{m}$ and $\lambda_1 = 9.091 \mu\text{m}$. Two different series of minimum reflectivity are obtained at depths h_m , where $m = 1, 2, 3$. These depths coincide with the resonant excitation of surface waves. The difference between two successive depths $h_{m+1} - h_m$ is equal to half-wavelength of the standing wave-coupled SPPs inside the cavity λ^{SW} .¹⁹ For an incident wavelength $\lambda = \lambda_0$, we obtained $\lambda^{\text{SW}} = 7.1 \mu\text{m}$ while for $\lambda = \lambda_1$, it increases to $7.5 \mu\text{m}$. To support the model of coupled SPPs inside the cavity, we solved the characteristic equation of a slab waveguide for an air gap between two semi-infinite SiO₂ layers.²⁴ The wave number of the coupled surface wave is calculated as

$$\beta = \left\{ k_0^2 + \frac{2}{\epsilon^2 d^2} [1 + \sqrt{1 + k_0^2 \epsilon^2 d^2 (1 + \epsilon)}] \right\}^{1/2}, \quad (1)$$

where k_0 is the wave number of the incident wave in a vacuum, and $d = \Lambda(1 - q) \approx 4.1 \mu\text{m}$ is the air gap of the cav-

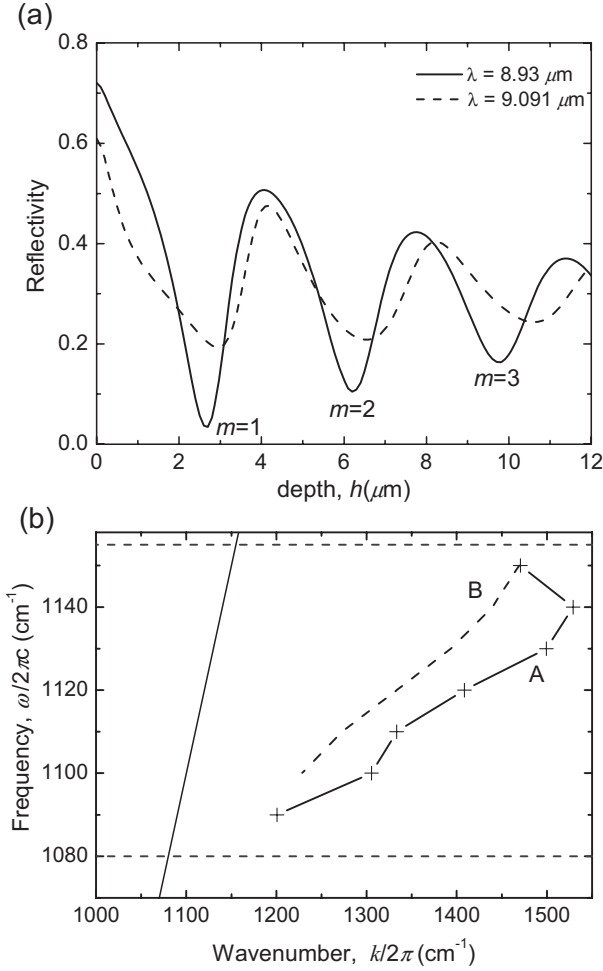


FIG. 2. (a) Calculated reflectivity of SiO₂-CRCs as a function of the cavity depth for incident wavelengths $\lambda_0=8.9 \mu\text{m}$ and $\lambda_1=9.091 \mu\text{m}$, at normal direction for TM states. (b) Dispersion relation of (A) standing wave coupled SPPs inside the resonant cavity, derived from the reflectivity calculation and (B) slab waveguide, derived from Eq. (1). The solid line depicts the light-line and the horizontal dashed lines represent the spectral range where $\epsilon' < -1$.

ity. Equation (1) is valid under the approximation that $d \ll 2\delta_{\text{air}}$ where δ_{air} is the decay length of the SPPs in air, which is evaluated by $\delta_{\text{air}} \approx 1/|\text{Im}\sqrt{k_0^2 - k_{\parallel}^2}| \approx 2.41 \mu\text{m}$. Figure 2(b) shows the dispersion curve of the standing wave-coupled SPPs derived from the analysis of reflectivity vs cavity depth (curve A) along with the calculated waveguide mode wave number given by Eq. (1) (curve B). There is a reasonable agreement between these curves, which supports the assumption that standing waves inside the cavities originate from an interaction between the decaying fields of SPPs on the cavity walls. In addition, one can notice that the slope of the dispersion curve is moderate, which corresponds to high DOS inside the cavity. We further confirm the standing wave-coupled SPPs mechanism by calculating the field distribution inside the cavities using a finite-difference time-domain algorithm. The magnitude of the transverse electric field $|E_x|$ in the x - z plane over a period is shown in Figs. 3(a)–3(c) for each resonant cavity depth h_m . Standing waves are discerned inside the cavity in the z direction with $m-1$

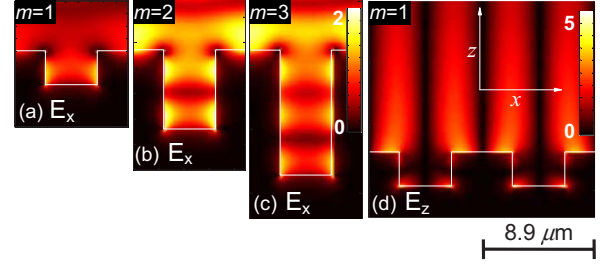


FIG. 3. (Color online). (a)–(d) The electric field distribution in the x - z plane at different resonant cavity depths h_m for incident wavelength λ_0 ; (a)–(c) $|E_x|$ at $m=1, 2$, and 3 , respectively, and (d) $|E_z|$ at h_1 .

nodes along the cavity walls. The maximum value of the electric field is obtained on the cavity walls and decays exponentially perpendicular to the walls into the cavity, which is typical of coupled surface waves behavior. The magnitude of the electric field is enhanced by a factor of 5 at the first resonance $m=1$ when the incident field is normalized, which verifies the high DOS of the localized mode. Increasing the DOS within the cavity can also be explained by the enhancement of the Purcell factor $F \propto Q/V_{\text{mod}}$, where V_{mod} is the modal volume. The total loss from the cavity is equal to the sum of the radiation into the free-space and scattering to the delocalized SPPs, hence a total Q can be expressed as $Q^{-1} \approx Q_{\text{rad}}^{-1} + [Q_{\text{SPPs}}/(1 + \cos \Delta\phi)]^{-1}$. $\Delta\phi$ is the phase difference between the scattering wave from the cavity and reflected waves from adjacent cavities.²⁵ For obtaining high Q (high DOS), destructive interference $\Delta\phi \sim \pi$ is required. The dark fringes shown in Fig. 3(d) indicate the behavior of this mechanism in our structure.

In order to excite directional emission, the localized modes should be correlated. One way to correlate adjacent cavities is by tunneling through the SiO₂ cavity walls. This correlation can be achieved if the penetration depth in the matter δ_{SiO_2} is sufficiently large compared with the distance between neighboring cavities $q\Lambda$. In case the distance between adjacent cavity walls is too large to enable tunneling (as in our case, $\delta_{\text{SiO}_2} \approx 0.66 \mu\text{m} \ll q\Lambda \approx 4.8 \mu\text{m}$), a different channel is required. As can be seen in Fig. 3(d), a horizontal standing wave exists on the surface between the cavity edges. This wave correlates adjacent resonant cavities while standing wave-coupled SPP correlates between adjacent ridges. The interplay between these mechanisms enables correlation of the electric field for long distance.²¹ The nonradiative horizontal standing wave is coupled to a radiative field by subtracting a discrete parallel momentum package of $K_g = 2\pi/\Lambda$ from the nonradiative wave's momentum according to $k_{\text{rad}} = k_{\text{HSW}} - K_g$, in order to reduce it into the light-line, where k_{HSW} is the horizontal standing wave number. At the resonant frequency ω_0 we obtained $k_{\text{HSW}} = \omega_0/c$, which is a noticeable different from delocalized SPP wave number $k_{\parallel} = 1.153\omega_0/c$. Our coupled resonant cavities behave as a coherent coupled thermal antennas. The analogy for the cavity is an infrared antenna consisting of a wire with a length of half-wavelength ($\lambda^{\text{SW}}/2$) at the operating frequency,²⁶ while coupling between these antennas produces the coherent emission.

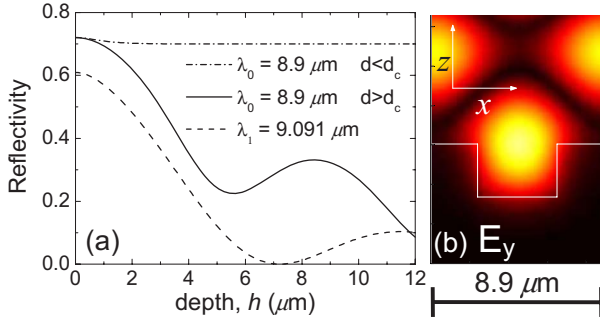


FIG. 4. (Color online). (a) Calculated reflectivity as a function of the cavity depth for incident wavelengths $\lambda_0=8.9 \mu\text{m}$ and $\lambda_1=9.091 \mu\text{m}$, at normal direction for TE polarization states (d_c is the cavity cutoff width for TE). (b) The field distribution $|E_y|$ in the x - z plane at resonant cavity depths h_1 for incident TE polarized wavelength λ_0 .

We now discuss the quasi-isotropic enhancement of thermal radiation at TE polarization state. This enhancement is due to the geometrical structure of the cavities and is not affected by its periodicity.²⁷ We have calculated the reflectivity as a function of the groove depth at incident TE polarized light for λ_0 and λ_1 . The results are shown in Fig. 4(a). As can be seen, at a groove depth of $2.7 \mu\text{m}$, the geometric resonance effect is minor compared to the coupled standing wave at TM polarization, hence the relative emissivity is smaller (~ 1.5). Note that as the grooves deepen, the geometric effect becomes the dominant mechanism for enhanced emission. The modulation of the reflectivity reveals coupling between the incident light and standing waves inside the cavities. This resonant wave is a guided mode which exists as long as the groove width d is higher than the cutoff width d_c . For an infinite waveguide, d_c is calculated from $d_c \approx \lambda/\pi \tan^{-1}(\sqrt{-\epsilon'})$,²⁸ to be $\sim 3 \mu\text{m}$. When the reflectivity is calculated for $d=1 \mu\text{m} < d_c$ no modulation is observed [see Fig. 4(a)] and the emissivity remains the same as that of a flat surface.¹⁷ A cross section of the field distribution over a period is shown in Fig. 4(b), demonstrating an enhanced localized field centered inside the cavity. Along the interface, the field is null since there are no surface waves. This distribution supports the behavior of broad angular emission for TE, as shown in Fig. 1(b).

Finally, we verified the generality of the CRC mechanism by investigating the coherency behavior of our structure upon crystalline polar material such as SiC. This material has a large coherence length of the delocalized surface waves characterized by $L_c \approx 1/\text{Im}(k_{\parallel})=55\lambda$ (at $\lambda=11.6 \mu\text{m}$). Figures 5(a) and 5(b) show the calculated spectral and angular emissivity of CRCs along with the results of a shallow grating for the TM polarization state. An extraordinary spatial coherence is obtained for the CRC structure $l_c \approx 440\lambda = 5.1 \text{ mm}$, which is higher by almost an order of magnitude compared with the coherency obtained by delocalized surface waves coupling mechanism. Moreover, enhanced temporal coherence is achieved, having a quality factor of Q

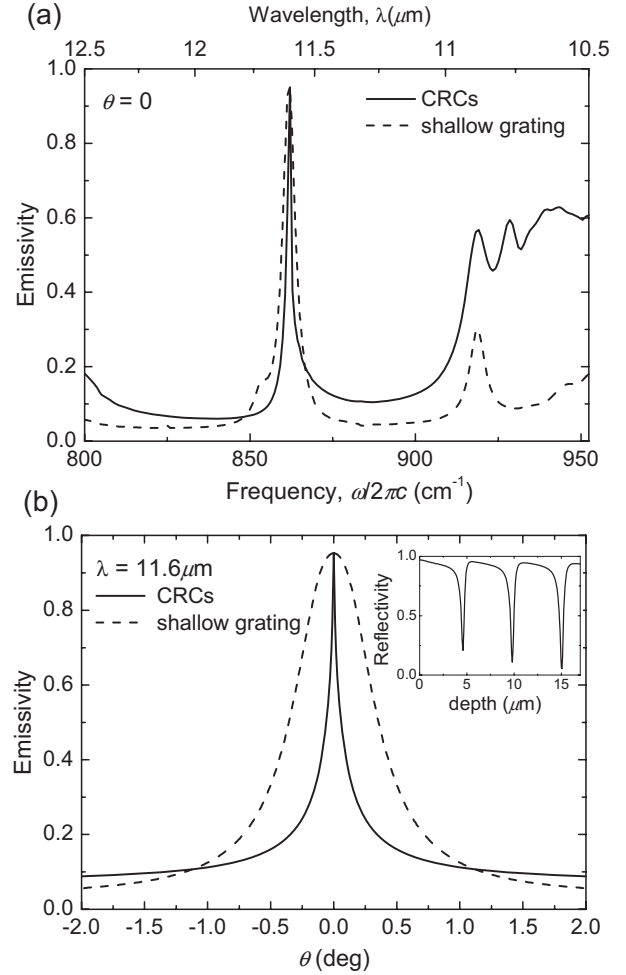


FIG. 5. Calculated emissivity of a SiC-CRC structure and of a shallow grating for TM polarized field as a function of (a) the emitted wavelength at normal direction and (b) the observed angle at $\lambda=11.6 \mu\text{m}$. The CRC parameters $\Lambda=11.6 \mu\text{m}$, $q=0.5$, and $h=15 \mu\text{m}$; the shallow grating parameters $\Lambda=11.36 \mu\text{m}$, $q=0.5$, and $h=0.3 \mu\text{m}$. The inset in (b) shows the reflectivity of CRCs vs cavity depth.

≈ 500 . The high Q resonant Fabry-Perot signature of the cavities is shown in the reflectivity vs cavity depth calculation [see inset in Fig. 5(b)], where very sharp dips are observed.

III. CONCLUSION

In conclusion, coupled resonant cavities enable high photonic DOS due to the resonant localized surface mode inside the cavities, along with coherent coupling with a high Q into a radiative field. An extraordinarily coherent thermal radiation that was not limited by the coherence length of the delocalized surface waves was obtained by means of a significant modification of the light-matter interaction by the CRCs. We demonstrated this key role on amorphous silica and crystalline SiC. Further investigation is required to elucidate the physical limitations of the coherence length for coupled resonant cavity structures.

- ¹J. B. Pendry, *J. Phys.: Condens. Matter* **11**, 6621 (1999).
- ²Y. De Wilde, F. Formanek, R. Carminati, B. Gralak, P.-A. Lemoine, K. Joulain, J.-P. Mulet, Y. Chen, and J.-J. Greffet, *Nature (London)* **444**, 740 (2006).
- ³A. Kittel, W. Müller-Hirsch, J. Parisi, S.-A. Biehs, D. Reddig, and M. Holthaus, *Phys. Rev. Lett.* **95**, 224301 (2005).
- ⁴L. D. Landau and E. M. Lifshitz, *Statistical Physics* (Pergamon Press, Exeter, 1980).
- ⁵S. M. Rytov, Y. A. Kravtsov, and V. I. Tatarskii, *Principles of Statistical Radiophysics* (Springer-Verlag, Berlin, 1989).
- ⁶A. V. Shchegrov, K. Joulain, R. Carminati, and J.-J. Greffet *Phys. Rev. Lett.* **85**, 1548 (2000).
- ⁷R. Carminati and J.-J. Greffet, *Phys. Rev. Lett.* **82**, 1660 (1999).
- ⁸T. Setälä, M. Kaivola, and A. T. Friberg, *Phys. Rev. Lett.* **88**, 123902 (2002).
- ⁹J.-J. Greffet, R. Carminati, K. Joulain, J.-P. Mulet, S. Mainguy, and Y. Chen *Nature (London)* **416**, 61 (2002).
- ¹⁰M. Laroche, C. Arnold, F. Marquier, R. Carminati, J.-J. Greffet, S. Collin, N. Bardou, and J.-L. Pelouard, *Opt. Lett.* **30**, 2623 (2005).
- ¹¹M. Trigo, A. Bruchhausen, A. Fainstein, B. Jusserand, and V. Thierry-Mieg, *Phys. Rev. Lett.* **89**, 227402 (2002).
- ¹²W. L. Barnes, A. Dereux, and T. W. Ebbesen, *Nature (London)* **424**, 824 (2003).
- ¹³Lord Rayleigh, *Theory of Sound* (Dover Publications, New York, 1945).
- ¹⁴H. A. Bethe, *Phys. Rev.* **66**, 163 (1944).
- ¹⁵R. W. Rendell and D. J. Scalapino, *Phys. Rev. B* **24**, 3276 (1981).
- ¹⁶E. D. Palik, *Handbook of Optical Constants of Solids* (Academic Press, Orlando, 1985).
- ¹⁷N. Dahan, A. Niv, G. Biener, V. Kleiner, and E. Hasman, *Appl. Phys. Lett.* **86**, 191102 (2005).
- ¹⁸E. Wolf, *J. Opt. Soc. Am.* **68**, 6 (1978).
- ¹⁹M. B. Sobnack, W. C. Tan, N. P. Wanstall, T. W. Preist, and J. R. Sambles, *Phys. Rev. Lett.* **80**, 5667 (1998).
- ²⁰J. A. Porto, F. J. García-Vidal, and J. B. Pendry, *Phys. Rev. Lett.* **83**, 2845 (1999).
- ²¹S. Collin, F. Pardo, R. Teissier, and J.-L. Pelouard, *Phys. Rev. B* **63**, 033107 (2001).
- ²²A. A. Maradudin, A. V. Shchegrov, and T. A. Leskova, *Opt. Commun.* **135**, 352 (1997).
- ²³H. Sai, Y. Kanamori, K. Hane, and H. Yugami, *J. Opt. Soc. Am. A* **22**, 1805 (2005).
- ²⁴F. Yang, J. R. Sambles, and G. W. Bradberry, *Phys. Rev. B* **44**, 5855 (1991).
- ²⁵Y. Akahane, T. Asano, H. Takano, B.-S. Song, Y. Takana, and S. Noda, *Opt. Express* **13**, 2512 (2005).
- ²⁶P. Mühlischlegel, H.-J. Eisler, O. J. F. Martin, B. Hecht, and D. W. Pohl, *Science* **308**, 1607 (2005).
- ²⁷P. J. Hesketh, J. N. Zemel, and B. Gebhart, *Nature (London)* **324**, 549 (1986).
- ²⁸R. Gordon and A. G. Brolo, *Opt. Express* **13**, 1933 (2005).